Supplementary Material

S1. Derivation of the inter-annual REOF ozone climatology.

An inter-annual global climatology of monthly zonal mean profile ozone is constructed by combining MLS profile ozone with SBUV total ozone and tropical zonal winds using a rotated EOF method as noted in section 4. The time length of this time-dependent climatology is 1970-recent.

We begin by deriving EOF vectors $\hat{e}_1(p), \hat{e}_2(p), ..., \hat{e}_{30}(p)$ and corresponding EOF coefficient time series $C_1(t)$, $C_2(t)$, …, $C_{30}(t)$ within each 5° latitude band from MLS monthly zonal-mean anomalies for 1-261 hPa (see Eq. (S1) below). Here, t represents month index (144 months for January 2005 – December 2016), p is pressure index (1-30), and the caret symbols mean that the EOF vectors are orthonormal. We used partial ozone pressure for the EOF analysis rather than ozone mixing ratio; by using partial pressure we found that we could use simple TOZ measurements to explain the first coefficient time series $C_1(t)$ at all latitudes.

The EOF analysis was done independently for each 5-degree latitude bin. Because all calculations are done for each latitude bin independently, we do not list latitude as a variable in the following equations in effort to simplify nomenclature. With 30 grid points (i.e., 30 pressure levels) for each EOF calculation within each 5° band, there are exactly 30 EOFs and 30 corresponding coefficient time series $C_n(t)$:

$$\mathrm{MLS}(p,t) \equiv \sum_{K=1}^{30} \hat{e}_K(p) \cdot C_K(t) \qquad \text{(S1)}$$

We note that the summation of all 30 components in Eq. (S1) exactly reproduces the original MLS ozone partial pressure profile measurements. As in Kutzbach (1967), we order the EOFs by the fraction of the total variance in the data explained by the respective EOF.

Figure S1 shows that the first two EOFs together explain from 65% and up to 85% of total variance of MLS ozone profile anomalies. We retain only these first two leading EOFs, as adding more EOF components to explain more of the variance increases complexity in describing and attributing the coefficients $C_K(t)$. Our analysis shows that the EOF1 coefficient $C_1(t)$ is highly correlated at all latitudes with TOZ time series. We also find that the EOF2 coefficient $C_2(t)$ in the tropics is largely explained by the QBO zonal winds.

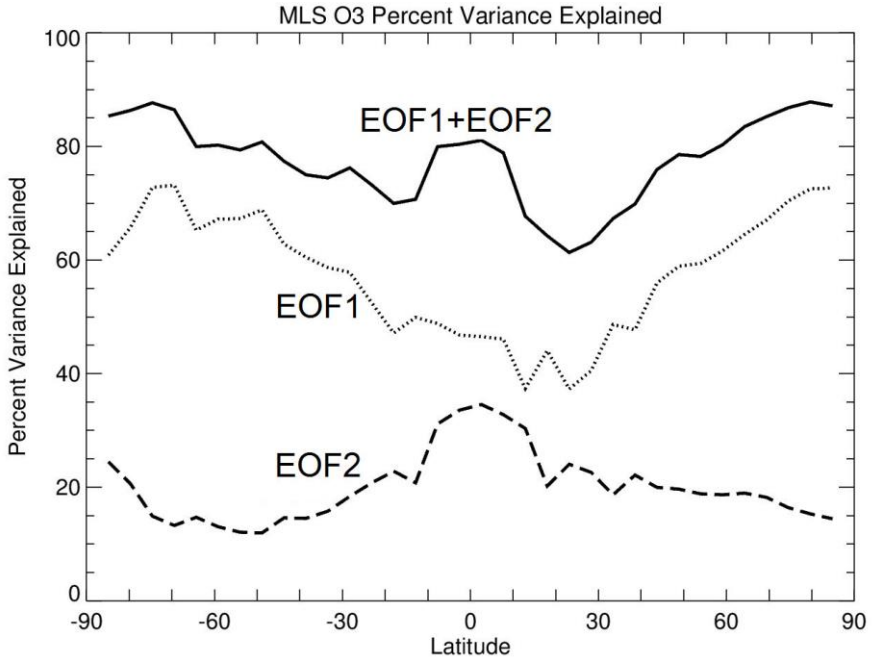

Figure S1. Total variance of MLS monthly zonal-mean de-seasonalized profile ozone (1-261 hPa) explained by the first and second leading EOFs, and their sum, as a function of latitude. The top curve shows that EOF1 and EOF2 together explain from 65% (NH low latitudes) up to 85% (both polar regions) of total variance.

Next, for each 5^o latitude band and using only the first two leading EOFs, we vertically integrate the resulting ozone profiles (right-hand side of Eq. (S1)) to derive a stratospheric ozone column SCO(t). We then apply a standard multiple linear regression (MLR) to explain time series of SCO(t) using the first two leading EOF coefficient time series $C_1(t)$ and $C_2(t)$:

$$\mathrm{SCO}(t) = a_1 \cdot \mathrm{C}_1(t) + a_2 \cdot \mathrm{C}_2(t) + \varepsilon(t) \qquad \text{(S2)}$$

where $\varepsilon(t)$ represents residual error of the regression.

Equation (S2) represents a rotated EOF expansion (e.g., Richman, 1986) for SCO(t) based on the two leading EOF coefficient time series C_1(t) and C_2(t) with a_1 and a_2 representing the derived regression constants. After calculating a_1 and a_2 from the regression, we then create a rotated EOF profile vector as follows:

$$\vec{E}_{rot}(p) = a_1 \cdot \hat{e}_1(p) + a_2 \cdot \hat{e}_2(p) \qquad \text{(S3)}$$

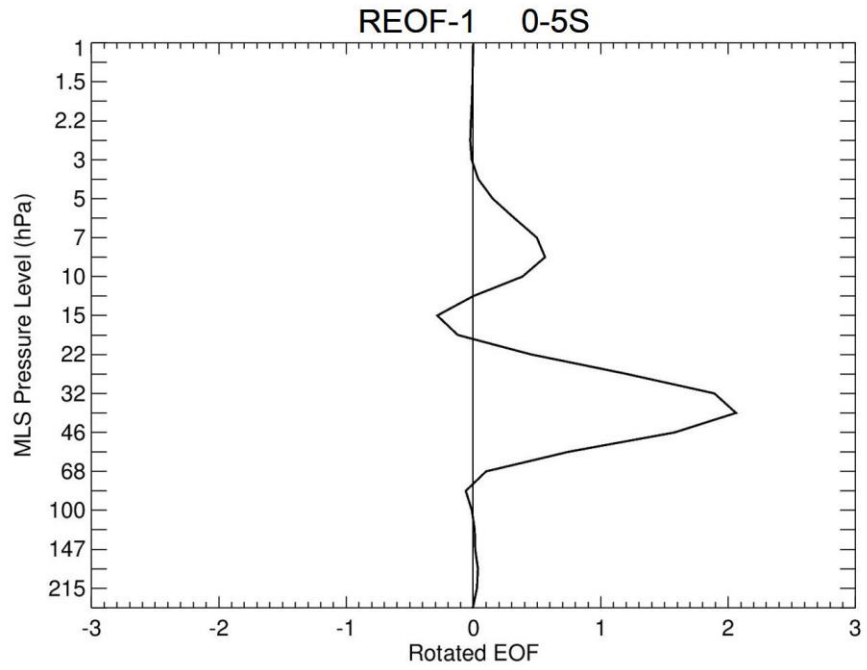

Figure S2. Example showing the rotated EOF profile vector REOF1 of ozone anomalies in the 0°-5°S latitude band derived from Eq. (S3).

An example of the rotated EOF vector REOF-1 for the latitude band 0°-5°S is shown in Fig. S2. The double-peak structure of REOF-1 with altitude in Fig. S2 is a characteristic of QBO dynamical forcing of ozone in the tropics.

After applying similar calculations for all 36 latitude bands, the global distribution for REOF-1 was derived and is shown in Fig. S3. The rotated EOFs in Fig. S3 generally have largest

amplitude in the low stratosphere with an exception in the NH polar region. The rotated EOFs have double peaked structures in the tropics and subtropics (originating from the QBO) and single peaked structures at higher latitudes.

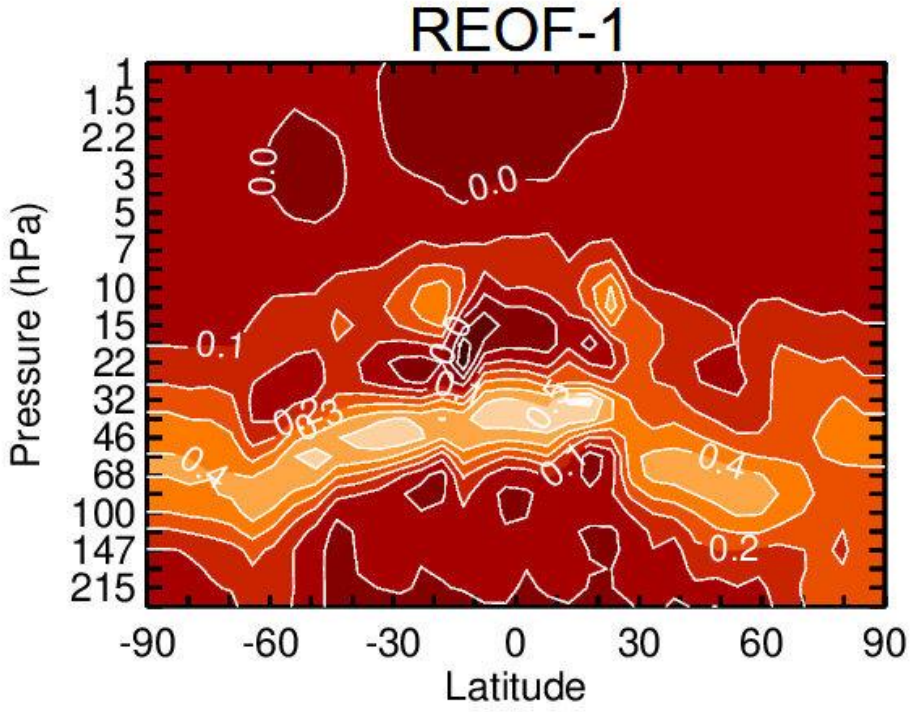

Figure S3. Vertical structures of REOF1 vectors derived from MLS monthly zonal mean deseasonalized ozone profiles for each of the 5° latitude bands 90°S-90°N.

For each latitude band the ozone profile can be reconstructed using the following equation (here X denotes ozone partial pressure)

$$X(p,t) = \vec{E}_{rot}(p) \cdot SCO(t) \qquad \text{(S4)}$$

In order to reconstruct ozone profiles for time periods before the lifetime of Aura, we use time series of monthly zonal mean total ozone anomalies of MOD TOZ(t) to replace SCO(*t*) in Eq. (S4). We did this since MOD total ozone covers the long time record from 1970-present and there is strong positive correlation between SCO and TOZ zonal-mean time series at all latitudes (i.e., correlations of +0.95 to +0.99 or greater. Equation (S4) then becomes:

$$\mathrm{X}(p,t) = \vec{\mathrm{E}}_{rot}(p) \cdot \mathrm{TOZ}(t) \qquad \text{(S5)}$$

However, neither a_1 nor a_2 in the earlier Eq. (S3) were normalized, so we must further adjust the profile climatology in (S5) such that the pressure-integrated profiles of ozone anomalies is as close as possible to the original MLS inter-annual SCO(t) time series for the time period August 2004 – December 2016. To do that, we apply a regression to the deseasonalized SCO from MLS and derive a regression normalization constant β as follows where $\mathrm{SCO_{MlS}}(t)$ represents measured MLS deseasonalized SCO(t):

$$\mathrm{SCO_{MLS}}(t) = \beta \cdot \int_{1hPa}^{261hPa} \vec{\mathrm{E}}_{rot}(p) \cdot \mathrm{TOZ}(t)\ dp + \varepsilon(t) \qquad \text{(S6)}$$

This yields then the profile climatology for ozone inter-annual anomalies that we call "step 1":

$$\mathrm{X_{STEP1}}(p,t) = \beta \cdot \vec{\mathrm{E}}_{rot}(p) \cdot \mathrm{TOZ}(t) \qquad \text{(S7)}$$

This step 1 climatology based on REOF1 explains a large fraction of ozone global inter-annual variability, however, the climatology can be improved in the tropics where there still remains some QBO variability that is not yet fully resolved in REOF-1 (S7). To further improve the inter-annual climatology in the tropics we derive EOF vectors and coefficient time series (in the same way as we did above), but now instead of using the de-seasonalized MLS ozone profiles, we use the residuals calculated by subtracting step-1 profile climatology Eq. (S7) from the de-seasonalized ozone anomalies.

The results show that the first leading EOF explains ~55% of the remaining variance in the tropics, which we found is related to the remaining QBO signal and can be explained almost entirely using the stratospheric zonal wind time series in the tropics. We thus retain only the first leading EOF profile vector $\hat{e}_1'(p)$ and corresponding first coefficient time series $\mathrm{C_1}'(t)$ to derive

a an additional "step-2" climatology of ozone profile anomalies that we will later add to the step-1 X_{STEP1} climatology (here, prime symbols denote step-2 EOF components).

Since we attributed $C_1'(t)$ to the QBO, we incorporate the rawinsonde monthly QBO winds to model $C_1'(t)$ in each 5° latitude band between 20°S and 20°N using linear regression as follows:

$$C_1'(t) = a_1 \cdot \mathrm{QBO}_1(t) + a_2 \cdot \mathrm{QBO}_2(t) + \varepsilon(t) \qquad \text{(S8)}$$

In (S8), $\mathrm{QBO}_1(t)$ and $\mathrm{QBO}_2(t)$ represent the two leading EOF coefficient time series for the equatorial zonal winds (e.g., Wallace et al. 1993), and a_1 and a_2 are derived regression constants. Following Wallace et al., (1993), an independent EOF analysis of the equatorial zonal winds in the stratosphere for pressure levels 10, 15, 20, 30, 40, 50, and 70 hPa was completed. We retained only the first two leading EOF time coefficients - $\mathrm{QBO}_1(t)$ and $\mathrm{QBO}_2(t)$ - because together the first two EOFs explain about 95% of total zonal wind variance. The step-2 ozone profile climatology in the tropics for 20°S-20°N can then be calculated as:

$$\mathrm{X}_{\mathrm{STEP2}}(p,t) = \hat{\mathrm{e}}_1'(p) \cdot [a_1 \cdot \mathrm{QBO}_1(t) + a_2 \cdot \mathrm{QBO}_2(t)] \qquad \text{(S9)}$$

The final REOF climatology of ozone profile inter-annual anomalies for 1970-present is then given by adding together step-1 climatology Eq. (S7) and step-2 climatology Eq. (S9):

$$\mathrm{X}_{\mathrm{CLIM}}(p,t) = \beta \cdot \vec{\mathrm{E}}_{rot}(p) \cdot \mathrm{TOZ}(t) + \hat{\mathrm{e}}_1'(p) \cdot [a_1 \cdot \mathrm{QBO}_1(t) + a_2 \cdot \mathrm{QBO}_2(t)] \qquad \text{(S10)}$$

S2. Analysis of the REOF inter-annual ozone climatology.

Figure 6 in the main text showed that inter-annual variability for the REOF climatology maximized not in the tropics (associated with dominant QBO) but instead in the SH extra-tropics. Figure S4 shows standard deviations calculated for a QBO-only climatology based on modeling MLS profile ozone with the QBO zonal winds by

$$\mathrm{MLS}(t) = a_1 \cdot \mathrm{QBO}_1(t) + a_2 \cdot \mathrm{QBO}_2(t) + \varepsilon(t) \qquad \text{(S11)}$$

where MLS(t) is ozone partial pressure (converted later to DU km^{-1}) and QBO$_1$(t) and QBO$_2$(t) are the EOF time coefficient time series of the QBO zonal winds just as in Eq. (S8). The long record for this climatology is determined by extrapolating backward in time prior to the MLS record by using the QBO EOF winds starting in 1970. We note that the standard deviations in the extra-tropics are substantially weaker for this QBO-only climatology compared to the final REOF climatology shown in Figure 6 of the main text.

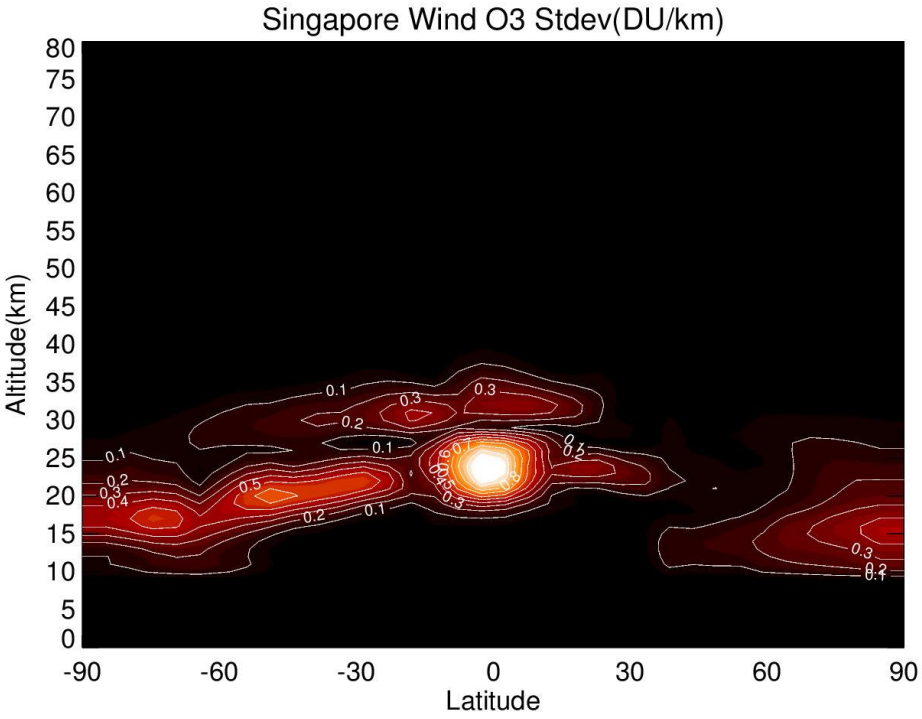

Figure S4. Temporal standard deviation (in DU km^{-1}) for a 1970-2018 ozone profile climatology based on only the QBO zonal winds as derived using Eq. (S11). The contour levels and coloring scale in this figure are the same as shown in Figure 6 of the main text.

In the tropics the QBO signal in stratospheric ozone exhibits large vertical gradients and a persistent downward phase propagation with time which is well reproduced with the REOF climatology. Figure S5 shows comparison of REOF profile ozone anomalies with deseasonalized monthly zonal mean profile ozone from SAGE II in the tropics (10°S-10°N) for 1984-2005. Despite SAGE being noisy due to sparse sampling (only a few days of zonal-mean measurements per month), the REOF and SAGE ozone anomalies compare generally well in time and space including sharp vertical gradients. Figure S6 shows a similar comparison between REOF and deseasonalized MLS ozone for years 2005-2018.

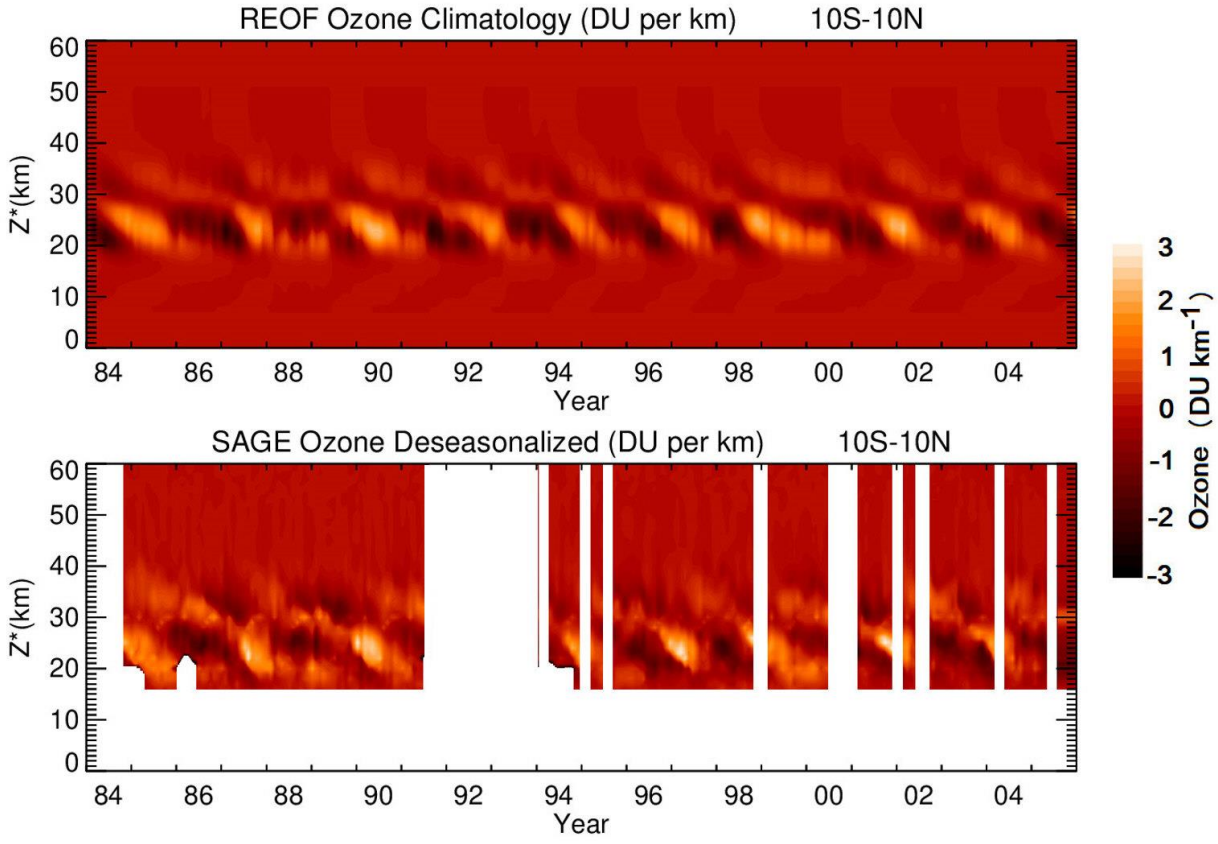

Figure S5. (top) REOF profile ozone inter-annual climatology (DU km^{-1}) plotted as log-pressure altitude (Z^*=0-60 km) versus month (1984-2005) in the tropics (10°S-10°N). Contours go from -3 (black) to +3 (white) in units DU km^{-1}. (bottom) Similar to (top), but instead for SAGE II deseasonalized profile ozone. The SAGE ozone in monthly values for 10°S-10°N is

noisy due to sparse sampling of SAGE with only a few days of measurements per month. The SAGE ozone measurements have been deleted for June 1991-December 1993 following the eruption of Mt. Pinatubo in June 1991. No smoothing is applied to any of the measurements.

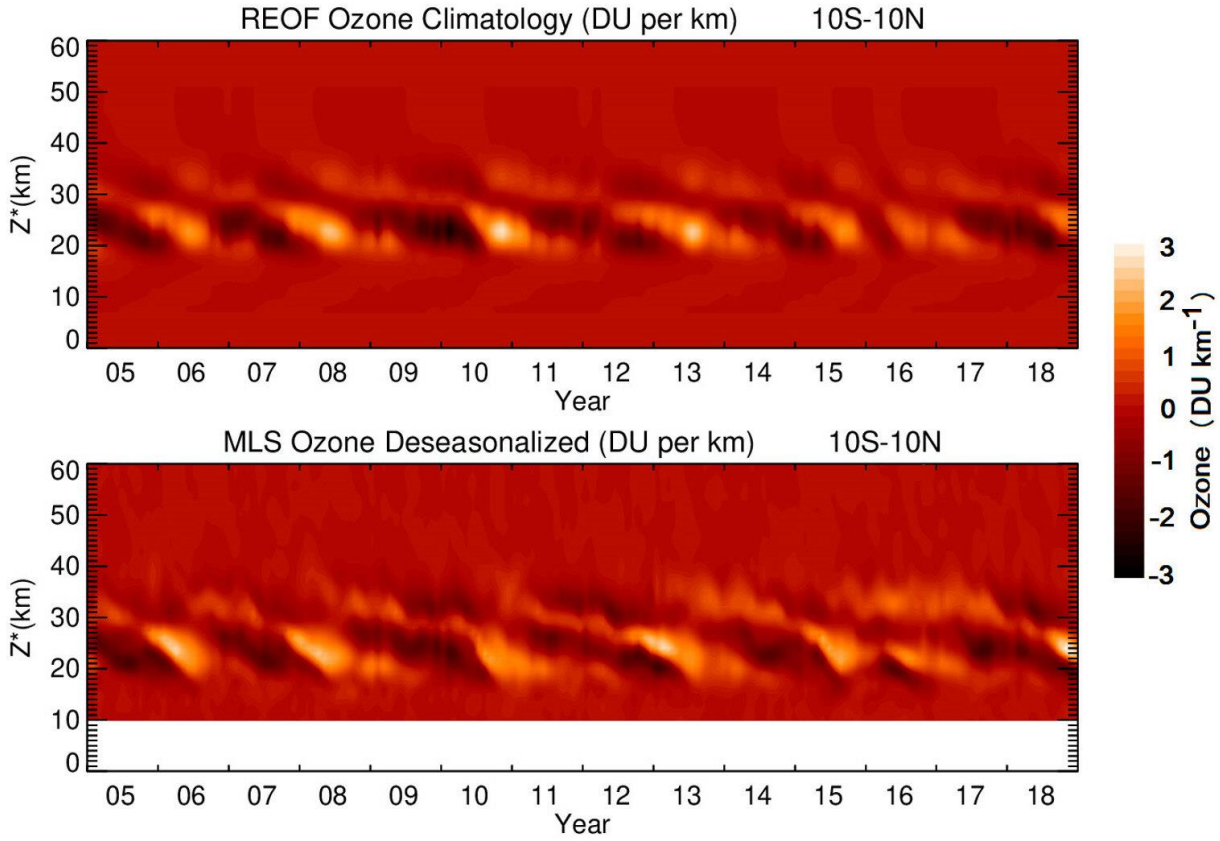

Figure S6. (top) REOF profile ozone climatology (DU km^{-1}) plotted as log-pressure altitude (Z^*=0-60 km) versus month (2005-2018) in the tropics (10^oS-10^oN). Contours go from -3 (black) to +3 (white) in units DU km^{-1}. (bottom) Similar, but instead for MLS deseasonalized profile ozone. No smoothing is applied to any of the measurements.

It is important to also compare REOF climatology meridional cross sections with SAGE II and MLS ozone meridional cross sections to evaluate how well they match up on a latitudinal basis.

193 Figure S7 shows several meridional cross section comparisons between REOF and SAGE II
194 ozone for selected months (indicated) when generally there is large variability in ozone present
195 in the extra-tropics. The sparse measurements from SAGE, often only 1 day of profiles per
196 month in a given 5^o latitude band produces serious aliasing effects whereby the zonal-mean
197 ozone profiles are not a good representation of true monthly averages. Figure S8 shows a similar
198 comparison between REOF and MLS ozone cross sections where the MLS does not have such a
199 poor sampling issue. The main conclusion from Figs. S7-S8 is that the REOF can capture a
200 substantial amount of inter-annual variability of ozone in the extra-tropics including months
201 when amplitudes are as large or larger than the QBO variability in the tropics.
202

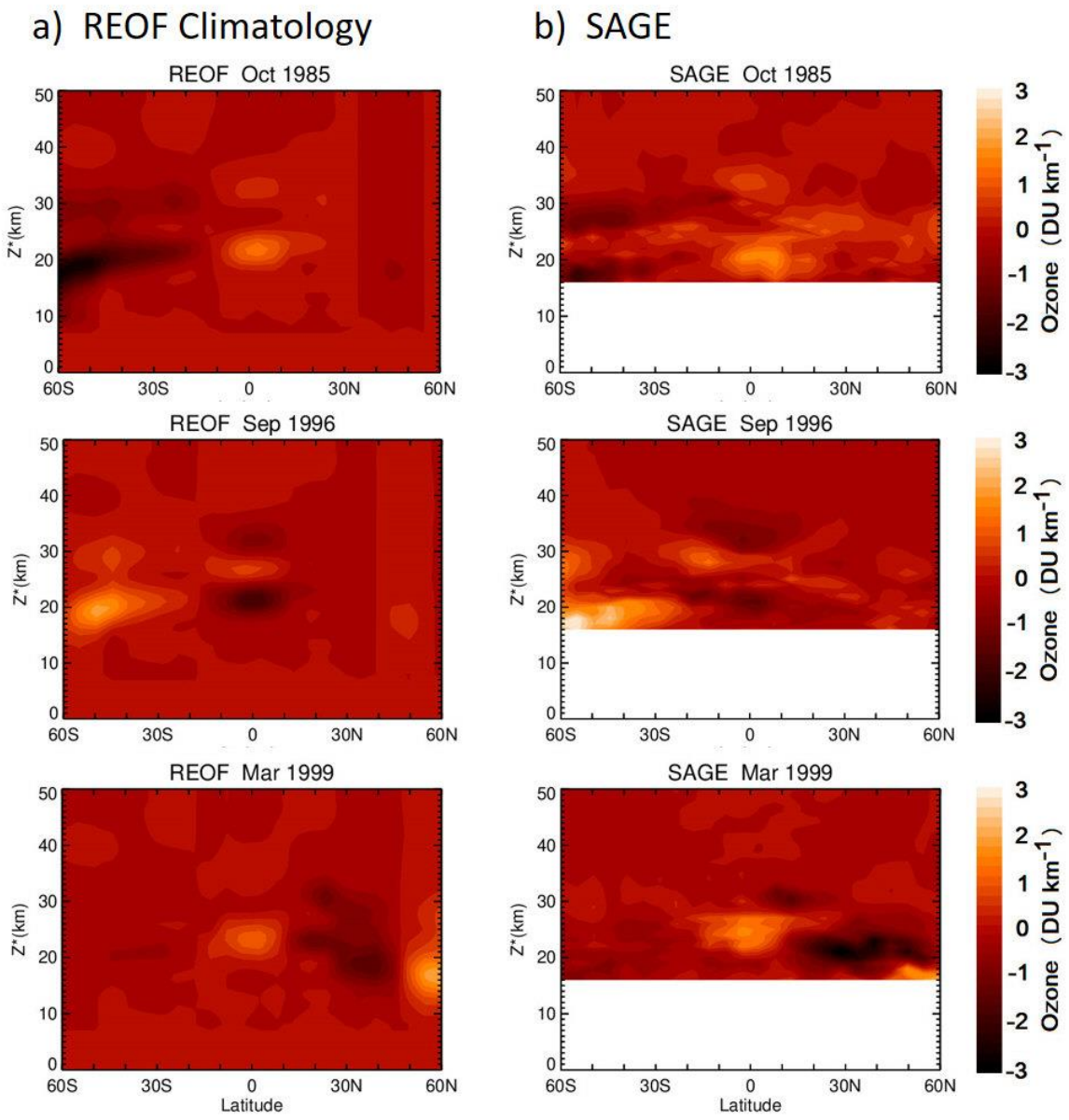

Figure S7. (a) The left-column panels show meridional height/latitude cross-sections of the REOF inter-annual ozone profile climatology at various months (indicated). (b) SAGE II deseasonalized zonal-mean ozone profiles are plotted to compare with the REOF meridional patterns in (a). All units are DU km^{-1}.

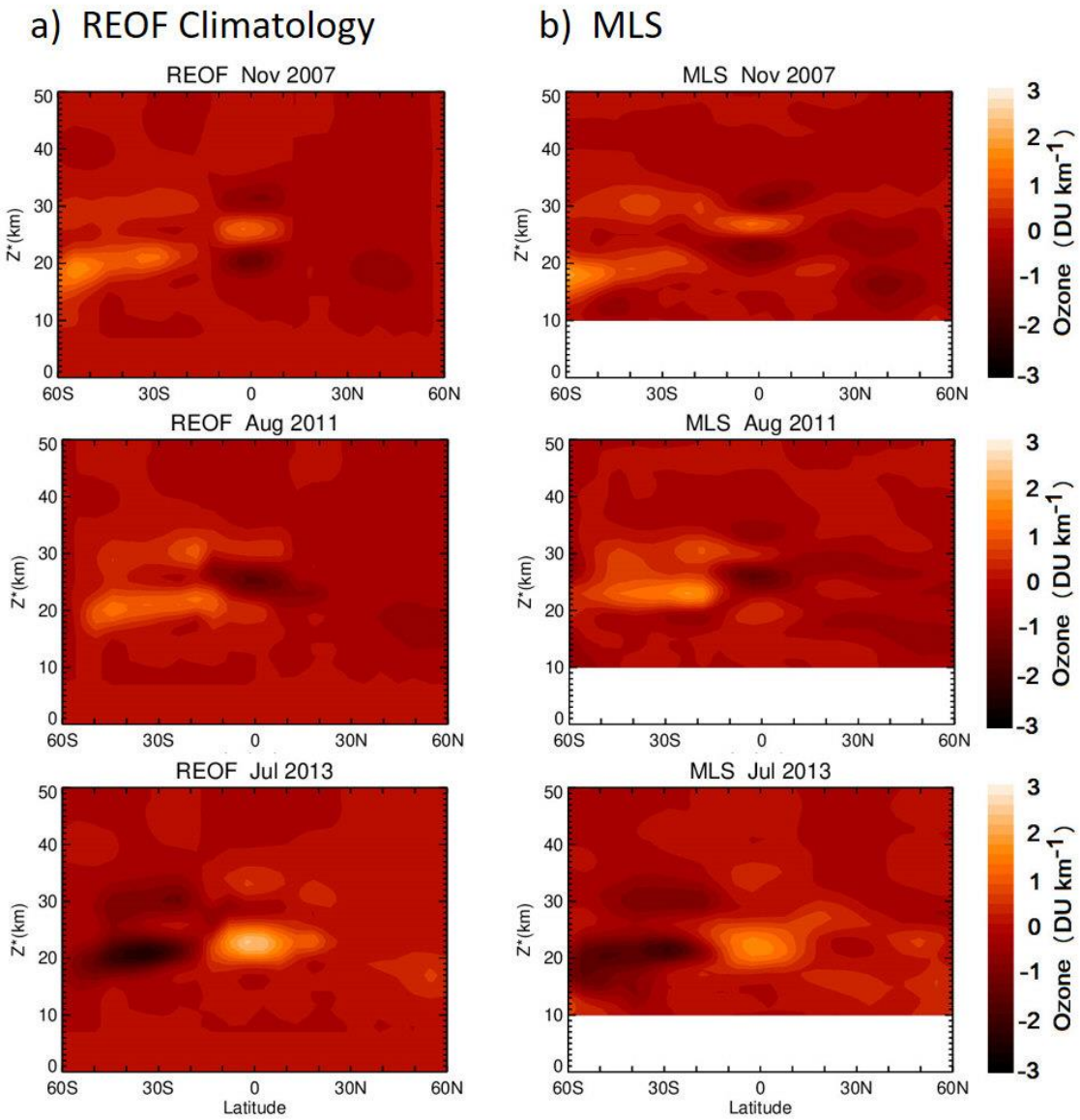

Figure S8. Same as Figure S7 but for REOF and MLS comparisons.

S3. Evaluation of M2GMI tropospheric ozone.

The M2GMI simulated tropospheric ozone has been extensively evaluated against measurements including satellites, sondes, lidars, and aircraft missions as discussed in section 2.4.1. Our study includes comparisons between M2GMI and lidar profiles as well as between M2GMI and ozonesonde columns and profiles. Figures 1-2 in the main text show examples of some of these

222 analyses. The ozonesonde database for our comparisons extends from 2004-2019 and includes
223 measurements from Southern Hemisphere ADditional OZonesondes (SHADOZ) (Thompson et
224 al., 2017; Witte et al., 2017), World Ozone and Ultraviolet Data Center (WOUDC)
225 (https://woudc.org/), and Network for the Detection of Atmospheric Composition Change
226 (NDACC). (http://www.ndsc.ncep.noaa.gov/). The ozonesondes provide daily ozone profile
227 volume mixing ratio as a function of altitude usually up to about 30-35 km in most cases. The
228 vast majority of the ozonesonde measurements are determined using Electrochemical
229 Concentration Cell (ECC) instruments.
230
231 Figure S9 compares TCO time series for 2005-2019 including M2GMI minus sonde differences
232 and standard deviations of their differences. For these monthly comparisons the offsets and
233 standard deviations are ~0-4 DU and 3-4 DU, respectively. The M2GMI ozone profiles were
234 also compared with sonde ozone profiles at selected Z* levels from 1-12 km (Fig. S10). In Fig.
235 S10 the M2GMI tropospheric ozone at each level in the troposphere captures much of global
236 variability of the ozonesondes with squared correlations of 0.6 to 0.9 (i.e., correlations +0.77 to
237 +0.95). When evaluated globally like this, the offset difference at any level in Fig. S10 is near
238 zero.
239
240 The M2GMI daily profile ozone in the troposphere was also compared with Lidar ozone profile
241 measurements from Table Mountain (43.7^{o}N, 110.8^{o}W) for 2004-2016 (Fig. S12). Fig. S12
242 shows calculated mean seasonal cycle comparisons of ozone mixing ratio between Lidar and
243 M2GMI for Z* = 2-9 km (1 km altitude steps). Ozone at Table Mountain in Fig. S12 throughout
244 the troposphere is largest in late spring which the M2GMI suggests is attributed to STE.
245 Interestingly, the ozone for 5-7 km for both Lidar and M2GMI exhibits a secondary maximum
246 around July-August period when annual recurring pollution is largest over N. America including
247 Table Mountain.
248
249
250
251

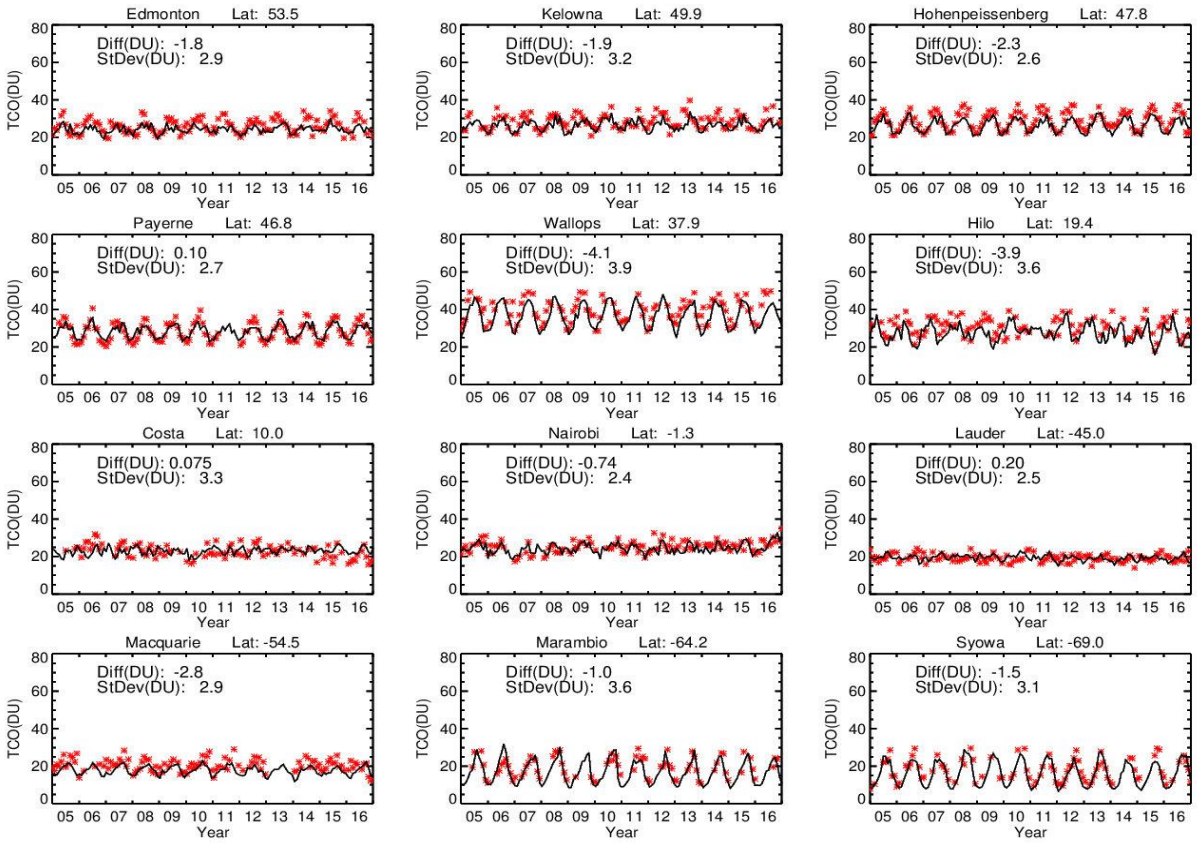

Figure S9. Monthly time series comparisons between M2GMI TCO (solid black curves) and ozonesonde TCO (red asterisks) for 2005-2019 at selected station sites from NH to tropics, to SH. All measurements of TCO are in Dobson Units. The monthly sondes represent a monthly ensemble of three or more daily measurements per month averaged together for these time series comparisons.

a)

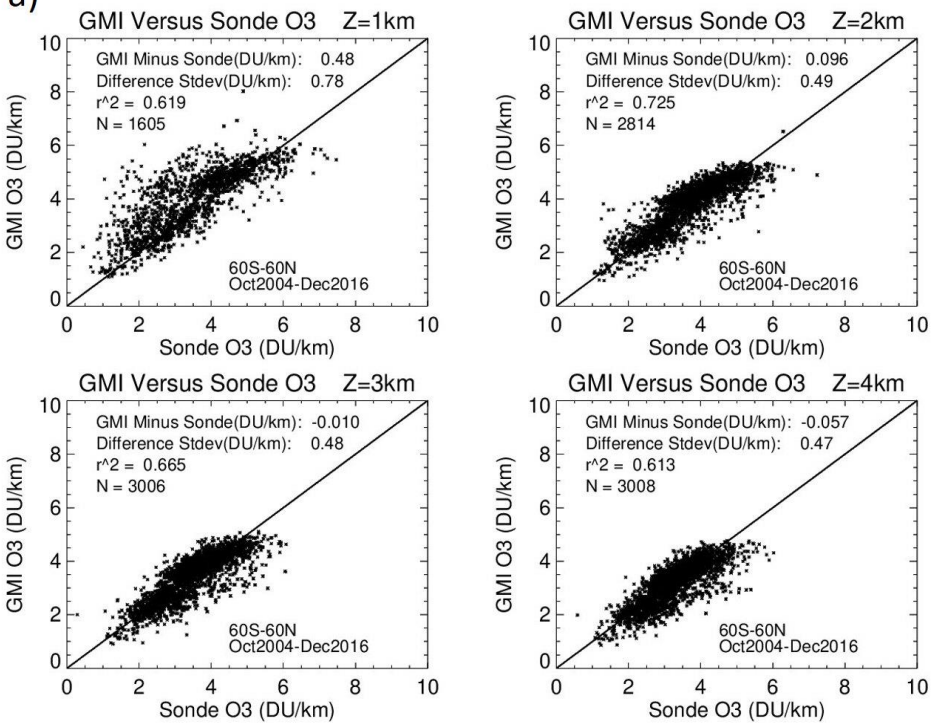

264

265

b)

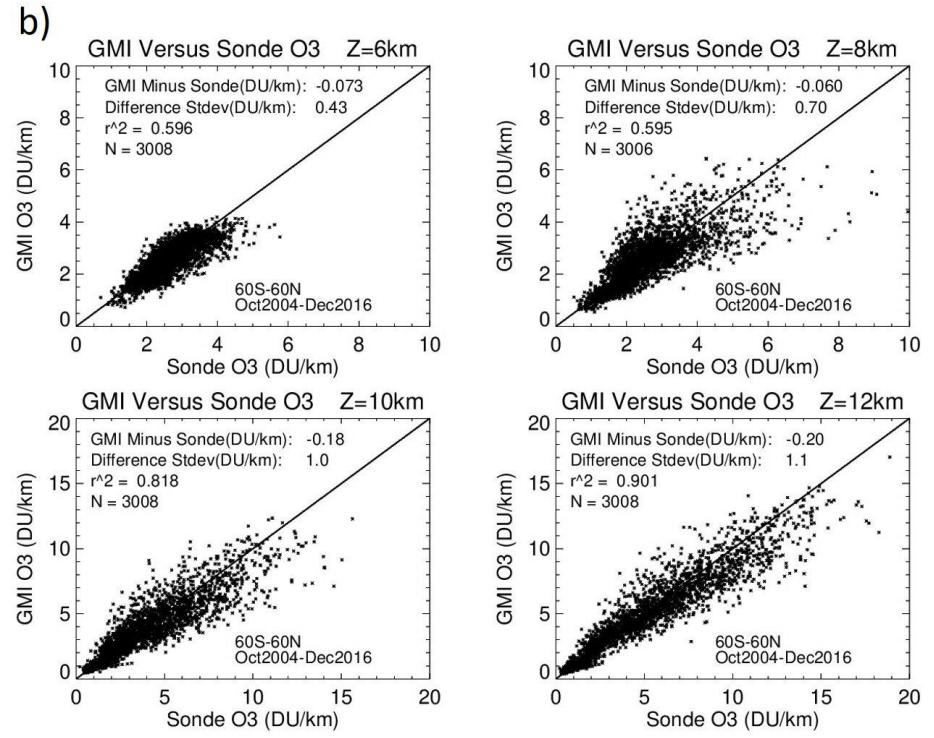

266

Figure S10. (a) Scatter diagrams of monthly-ensemble M2GMI ozone versus monthly sonde ozone for selected Z* altitudes (1, 2, 3, 4 km), accrued for all 40 stations for 60°S-60°N and time period October 2004-December 2016. Units for ozone are DU km^{-1}. Included in each panel are statistical mean differences, standard deviations, square of correlation, and total number of data pair matchups. (b) same as (a) but for Z* altitudes 6, 8, 10, 12 km. Monthly-ensemble ozone for M2GMI represents true monthly average whereas for sondes it represents at least 3 profile measurements averaged together per month.

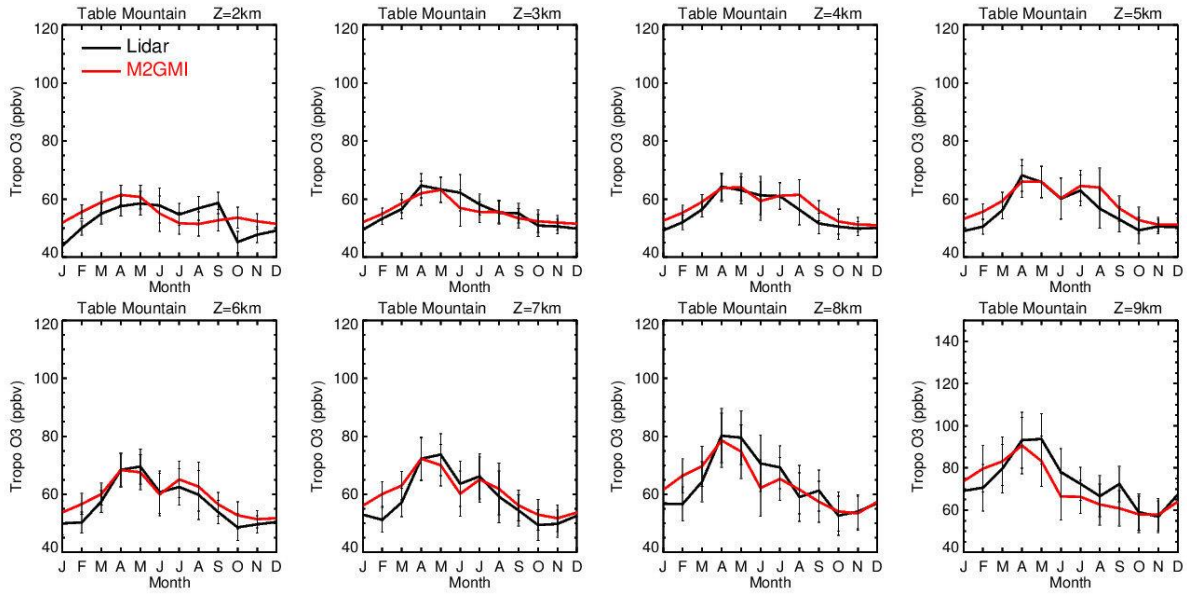

Figure S11. Twelve-month seasonal cycles of ozone volume mixing ratio (units ppbv) comparisons between M2GMI (red curves) and Lidar (black curves) at Table Mountain (43.7°N, 110.8°W) for selected vertical Z* levels of 2-9 km. All 12-month seasonal cycles were calculated from daily measurements averaged monthly for January 2004 – December 2016. Vertical bars represent ±1σ standard deviation.

S4. Additional material relating to the MLS/GMI seasonal climatology.

The follow figures relate to the MLS/GMI seasonal climatology (see figure captions for details). Figure S12 shows the MLS/GMI ozone mixing ratio climatology averaged over three-month

seasons (indicated) for Z^* altitudes 0-80 km and latitudes 90°S-90°N. The largest concentrations of ozone mixing ratio occur in the tropics around 35 km. Highest mixing ratio in the mesosphere above Z^* = 60 km exceeds 1 ppmv and occurs during winter in both polar regions. Figures S13-S14 show the calculated standard deviations for the MLS/GMI climatology as both units ppmv (Fig. S13) and percent of background ozone (S14).

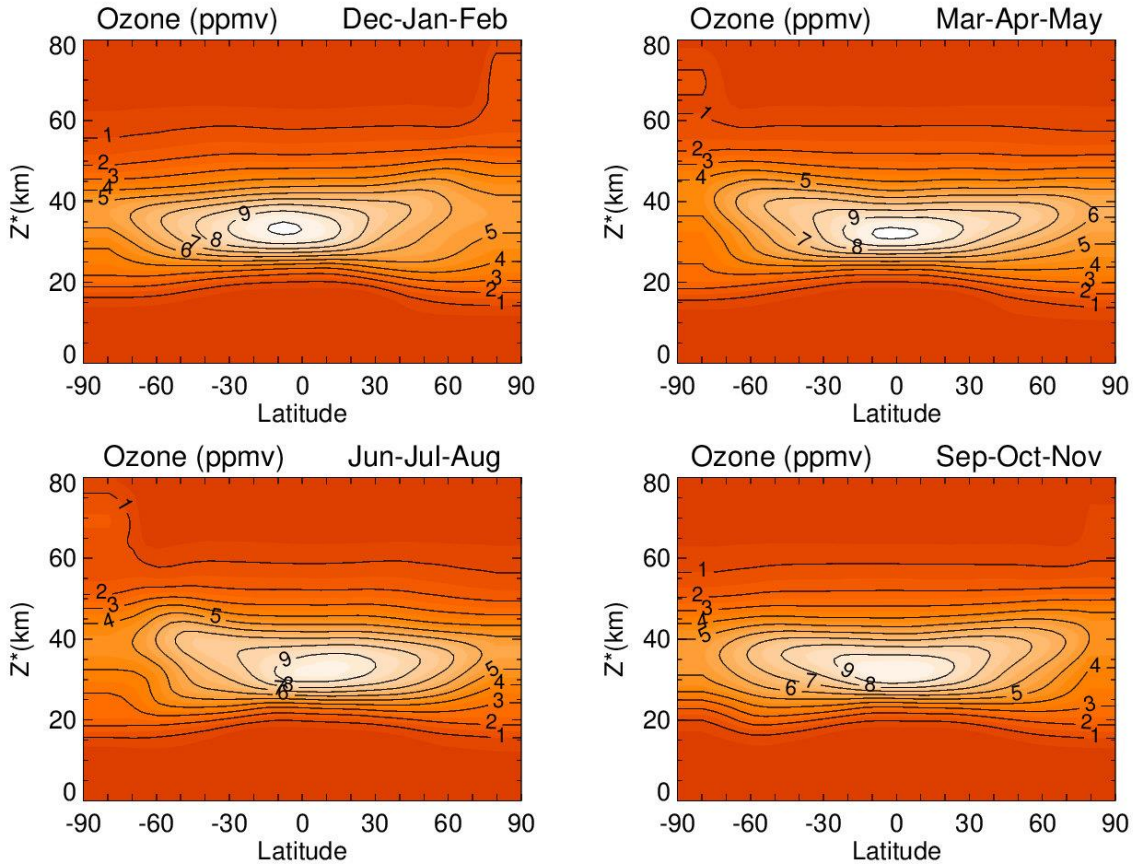

Figure S12. Meridional cross-sections of derived zonal-mean ozone volume mixing ratio profiles (units ppbv) for the MLS/GMI seasonal climatology. This 12-month climatology is averaged over three-month seasons (indicated) for 2004-2016 and is binned in 5° latitude bands for Z^* levels from 0-80 km at 1 km spacing (see main text).

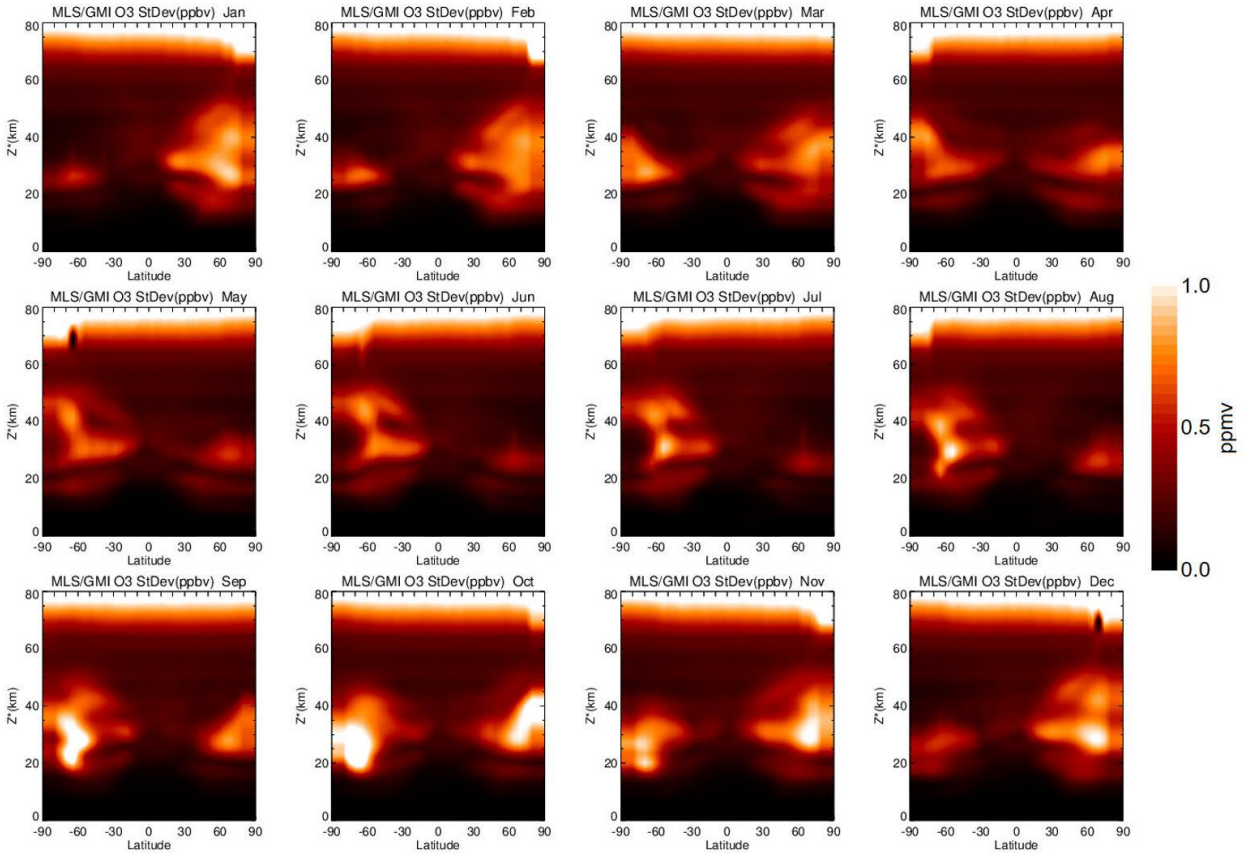

Figure S13. Meridional cross sections of the MLS/GMI climatology standard deviations of volume mixing ratio with units ppbv.

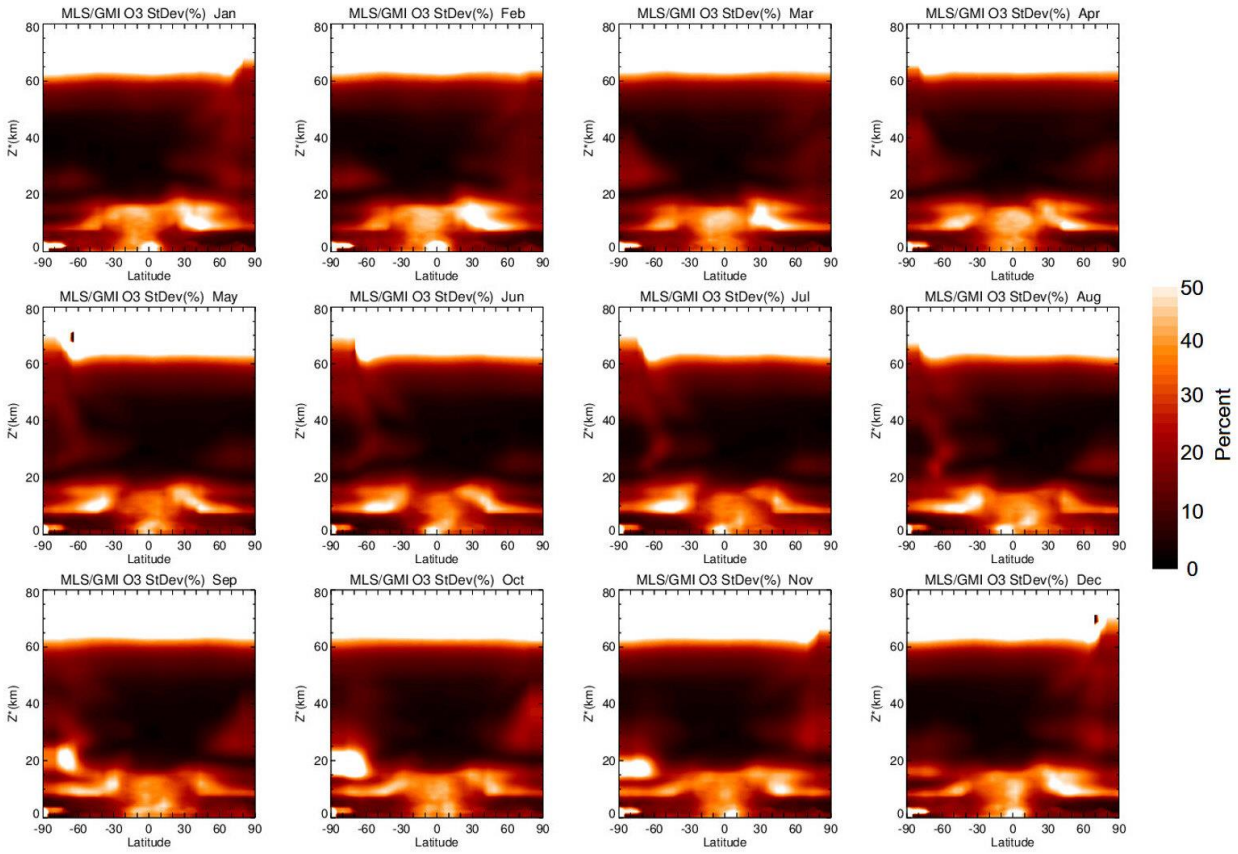

Figure S14. Similar to Fig. S15 but plotted as percentage of background monthly average climatology ozone volume mixing ratio.